X-ray and Sunyaev-Zel'dovich Effect cluster scaling relations: numerical simulations vs. observations

Daisuke Nagai

Theoretical Astrophysics, California Institute of Technology, Mail Code 130-33, Pasadena, CA 91125
daisuke@caltech.edu

1 Introduction

Clusters of galaxies are potentially powerful observational probes of the nature of dark energy. This has motivated construction of large multi-wavelength cluster surveys ranging from microwave, optical to X-ray. Upcoming cluster surveys are designed to detect many thousands of clusters, aiming to deliver significant observational constraints on the equation of state of dark energy. However, to realize the full statistical power of these experiments and to make interesting contribution for dark energy studies, the relationship between cluster mass and observables needs to be calibrated at a level of a few percent. This stringent requirement poses significant observational and theoretical challenges.

In this contribution, I will present theoretical work that complements ongoing and future observational efforts and describe high-resolution cosmological simulations of galaxy clusters that self-consistently follow cluster gas-physics and stellar feedback. We show that observable-mass relations for our simulated sample agree with the *Chandra* and SZE measurements to $\approx 10\%$ in normalization, which is a considerable improvement given that significant disagreement existed just several years ago. The remaining systematic difference could be caused by subsonic gas motions, unaccounted for in hydrostatic mass estimates. While further advances in our understanding of cluster physics are imperative for future dark energy studies, the much improved agreement of simulations and observations in the cluster scaling relations is encouraging and hold promise for the use of clusters as cosmological probes.

2 Cosmological Simulations of Galaxy Clusters

We present high-resolution cosmological simulations of 16 cluster-sized systems performed with the Adaptive Refinement Tree (ART) N-body+ gasdynamics code (Kravtsov 1999) in the concordance ΛCDM model. The ART code is an Eulerian code designed to achieve high spatial resolution by adaptively refining regions of interest, such as high-density regions, and has good shock-capturing characteristics. To assess the impact of galaxy formation, we compare two sets of simulations, one performed in the non-radiative regime and another with radiative cooling and several physical processes critical to various aspects of galaxy formation: star formation, metal enrichment and stellar feedback, which we refer to as the cooling+SF (CSF) model. The resolution of the simulations is sufficiently high to resolve formation and evolution of cluster galaxies and their impact on cluster gas. The simulations used 128^3 uniform grid and 8 levels of refinement, which corresponds to the peak resolution of 3-$5h^{-1}$kpc in the 80-$120h^{-1}$Mpc computational boxes. Simulated clusters are also resolved with more than a million dark matter particles. Physical processes that might significantly affect the properties of cluster core regions, such as AGN feedback, cosmic-rays, magnetic field, thermal conduction, and physical viscosity, are not included in the simulations presented in this work.
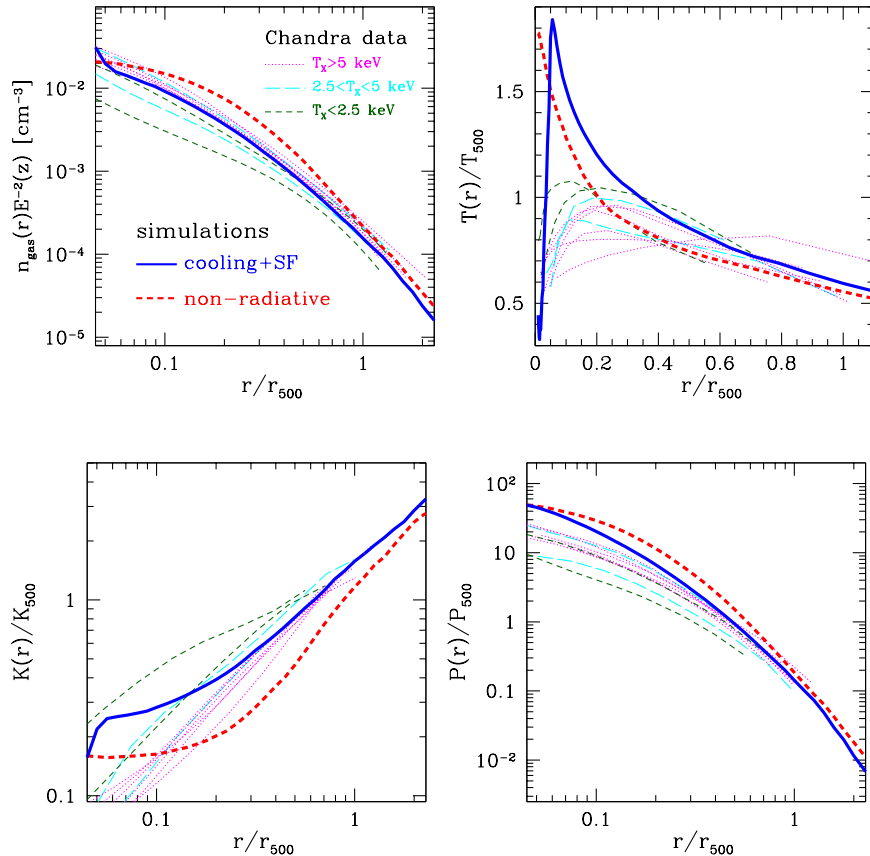
Fig. 1. Comparison of the ICM profiles in relaxed clusters at the present day ($z \approx 0$) in cosmological cluster simulations and the *Chandra* sample of Vikhlinin et al. (2006a). The panels show the gas density (*top-left*), temperature (*top-right*), entropy (*bottom-left*), and pressure (*bottom-right*). *Thick* solid and dashed lines show the mean profiles in the CSF and non-radiative simulations, respectively, while the observed profiles are shown by the *thin* dotted, long-dashed and short-dashed lines for the systems with $T_X > 5$ keV, $2.5 < T_X < 5$ keV, and $T_X < 2.5$ keV, respectively. Note that at $r \gtrsim 0.1 r_{500}$ the profiles of the CSF simulations provide a better match to the observed profiles than the profiles in the non-radiative runs. Reproduced from Nagai, Kravtsov, Vikhlinin (2007b).

In order to compare results of numerical simulations directly to observations as well as to assess systematic uncertainties in X-ray measurements, we generate mock *Chandra* images of the simulated clusters and analyze them using a model and procedure essentially identical to those used in real data analysis (Nagai et al. 2007a). For each cluster, the mock data is created for three orthogonal projections along the x, y, and z coordinate axes. The average X-ray spectral temperature, T_X, is obtained from a single-temperature fit to the spectrum integrated within r_{500}, excluding the central region, $r < 0.15 r_{500}$ (Mazzotta et al. 2004; Vikhlinin et al. 2006b). We also use total mass, gas mass as well as integrated cluster properties derived from the mock X-ray analysis for studies of cluster scaling relations in Section 4. Additional details of simulations and analysis of mock *Chandra* X-ray data can be found in Nagai et al. (2007a,b).

3 Effects of Galaxy Formation on the Properties of the ICM

We investigate effects of galaxy formation on the ICM properties and compare results of numerical simulations with recent deep *Chandra* X-ray observations of nearby relaxed clusters Vikhlinin et al. (2005,2006a), which are especially ideal for testing numerical simulations and
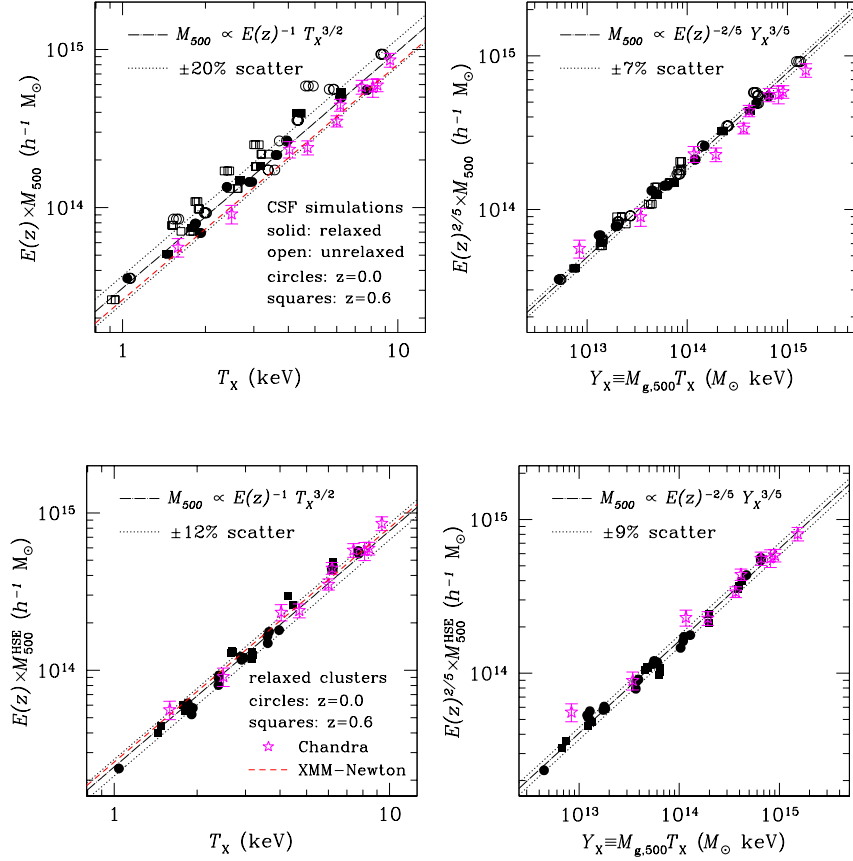
Fig. 2. Correlation between the total mass, M_{500c} and X-ray spectral temperature, T_X (*left panel*) and the integrated X-ray pressure, Y_X (*right panel*). Relations are shown for the true 3D cluster mass $M_{500} \equiv M(< r_{500}^{\mathrm{true}})$ as measured in simulations (*upper panels*) and the hydrostatic mass $M_{500}^{\mathrm{HSE}} \equiv M^{\mathrm{HSE}}(< r_{500}^{\mathrm{est}})$ derived from mock *Chandra* analysis (*lower panels*). Separate symbols indicate relaxed and unrelaxed simulated clusters, and also z=0 and 0.6 samples. The figures include points corresponding to three projections of each cluster. The *dot-dashed* lines are the power law relation with the self-similar slope fit for the sample of relaxed clusters. The *dotted* lines indicate the rms scatter around the mean relation. The data points with errorbars are *Chandra* measurements of nearby relaxed clusters. The *dashed* line is the best-fit M-T_X relation from the *XMM-Newton* measurements. Reproduced from Nagai, Kravtsov, Vikhlinin (2007b).

assessing effects of the input cluster physics. In Figure 1, we show the observed ICM properties outside cluster cores are well-reproduced in the simulations that include cooling and star formation. The inclusion of gas cooling and star formation modify both the normalization and the shapes of the ICM profiles. What happens is that removal of low-entropy gas via gas cooling and star formation in the inner region increases the entropy ($K \equiv T/n_e^{3/2}$), which is accompanied by the increase of temperature and decrease in gas density (Voit & Bryan 2001). The effects are strongly radial dependent and increase toward the inner regions down to about $r \lesssim 0.15 r_{500}$, inside which the observed properties are not well reproduced in the current simulations (indicating the need for additional cluster physics in simulations). At $r = r_{500}$, both the ICM density and entropy profiles of different mass systems converge, indicating that clusters are self-similar in the outskirts, and that outer regions of clusters can be used to reliably estimate their total mass.

4 X-ray and SZE observable-mass relations

In Fig. 2, we present comparisons of the X-ray observable-mass relations of the CSF simulations and *Chandra* and *XMM-Newton* X-ray observations of nearby relaxed clusters, focusing on two X-ray proxies for the cluster mass — the spectral temperature (T_X) and the X-ray pressure ($Y_X \equiv T_X M_g$).

The $M_{500} - T_X$ relation show fairly tight correlation with a slope close to the self-similar value. The scatter is $\sim 20\%$ in M_{500} around the mean relation, most of which is due to unrelaxed clusters. The normalization for our simulated sample agrees with both *Chandra* (Vikhlinin et al. 2006a) and *XMM-Newton* (Arnaud et al. 2005) measurements to $\approx 10\%$. This is a considerable improvement given that significant disagreement existed just several years ago (Finoguenov et al. 2001; Pierpaoli et al. 2003). The residual systematic difference in the normalization is likely caused by non-thermal pressure support from bulk gas motions, which is unaccounted for in hydrostatic mass estimates (Rasia et al. 2006; Dolag et al. 2006; Lau et al. 2008). For example, when we repeat the comparison of scaling relations using hydrostatic mass estimates for the observed clusters, we find excellent agreement in normalizations, demonstrating explicitly that there is a systematic $\approx 10\%$ offset between hydrostatic mass estimate and the true mass in simulated clusters. Note also that the unrelaxed clusters have temperatures biased low for a given mass, because only a fraction of the kinetic energy of merging systems is converted into the thermal energy of gas, due to incomplete relaxation during mergers (Mathiesen & Evrard 2001).

The $M_{500} - Y_X$ relation shows considerably smaller scatter of only $\approx 7\%$ (Kravtsov et al. 2006). Note that this value of scatter includes clusters at both low and high-redshifts and both relaxed and unrelaxed systems. In fact, the scatter in $M_{500} - Y_X$ for relaxed and unrelaxed systems is indistinguishable within the errors. Moreover, we find no systematic offset between the observed and model $M_{500} - Y_X$ relations among clusters in different dynamical states. Y_X is therefore a robust mass indicator with remarkably low scatter in M_{500} for fixed Y_X, regardless of whether the clusters are relaxed or not. The redshift evolution of the $Y_X - M_{500}$ relation is also close to the simple self-similar prediction, which makes this indicator a very attractive observable for studies of cluster mass function with X-ray selected samples, as it indicates that the redshift evolution can be parameterized using a simple, well-motivated function. If we use hydrostatic mass for comparisons, the observed and model relations are in excellent agreement (Nagai et al. 2007b; see also Arnaud et al. 2007).

The integrated SZE signal, Y_{SZ}, is directly proportional to the thermal energy content of the ICM – a robust cluster mass proxy. This indicates that the SZE survey will enjoy a remarkably simple and uniform selection function with redshift. Recent numerical simulations indicate that a very tight relation exists between Y_{SZ} and cluster mass, even when realistic cluster gas-physics are included in simulations (Motl et al. 2006; Nagai 2006). The amplitude of the relation, on the other hand, is sensitive to the cluster physics (Nagai 2006). Figure 3 shows comparisons of numerical simulations with 38 clusters ($0.14 < z < 0.89$) observed with *Chandra* and OVRO-BIMA (Bonamente et al. 2008). The comparison indicates that both sets of simulation models show a similar slope to the observed clusters, with the cooling and star formation feedback model providing a better match to the data. While further improvements in calibration of observable-mass relations are essential for future dark energy studies, the existence of tight relations of X-ray and SZE observables, such as Y_X and Y_{SZ}, and total cluster mass and the simple redshift evolution of these relations hold promise for the use of clusters as cosmological probes.
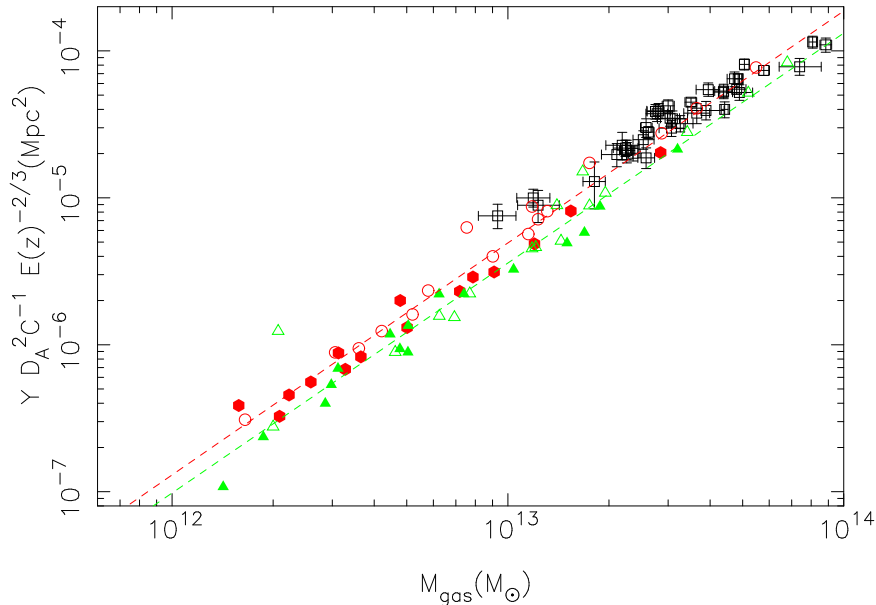
Fig. 3. Y_{SZ} vs. M_{gas} for simulated and observed clusters. Open squares (in black) are OVRO/BIMA/Chandra measurements. Also shown are simulated clusters from a cooling and star-formation feedback model (red circles) and simulated clusters from a non-radiative model (green triangles) from Nagai 2006. For comparison, all of the Y_{SZ} and M_{gas} quantities are integrated over a spherical volume. Open symbols represent simulated clusters at $z{=}0$ and filled symbols represent simulated clusters at $z{=}0.6$. Reproduced from Bonamente et al. (2008).

References

1. Arnaud, M., Pointecouteau, E., & Pratt, G. W. 2005, A&A, 441, 893
2. Arnaud, M., Pointecouteau, E., & Pratt, G. W. 2007, A&A, 474, 37
3. Bonemente, M., Joy, M., LaRoque, S., Carlstrom, J., Nagai, D., & Marrone, D. 2008, ApJ, to appear in February 20, v674n 2 issue (astro-ph/0708.0815)
4. Dolag, K., Vazza, F., Brunetti, G., & Tormen, G. 2005, MNRAS, 364, 753
5. Finoguenov, A., Reiprich, T. H., & Böhringer, H. 2001, A&A, 368, 749
6. Kravtsov, A. V. 1999, PhD thesis, New Mexico State University
7. Kravtsov, A. V., Vikhlinin, A., & Nagai, D. 2006, ApJ, 650, 128
8. Lau, E., Kravtsov, A. V., & Nagai, D. 2008, in preparation
9. Mathiesen, B. F. & Evrard, A. E. 2001, ApJ, 546, 100
10. Mazzotta, P., Rasia, E., Moscardini, L., & Tormen, G. 2004, MNRAS, 354, 10
11. Motl, P. M., Hallman, E. J., Burns, J. O., & Norman, M. L. 2005, ApJL, 623, L63
12. Nagai D., Vikhlinin A., Kravtsov A. V., 2007a, ApJ, 655, 98
13. Nagai D., Kravtsov A. V., Vikhlinin A., 2007b, ApJ, 668, 1
14. Nagai, D. 2006, ApJ, 650, 538
15. Pierpaoli, E., Borgani, S., Scott, D., & White, M. 2003, MNRAS, 342, 163
16. Rasia, E., Ettori, S., Moscardini, L., Mazzotta, P., Borgani, S., Dolag, K., Tormen, G., Cheng, L. M., & Diaferio, A. 2006, MNRAS, 369, 2013
17. Vikhlinin, A., Markevitch, M., Murray, S. S., Jones, C., Forman, W., & Van Speybroeck, L. 2005, ApJ, 628, 655
18. Vikhlinin, A., Kravtsov, A., Forman, W., Jones, C., Markevitch, M., Murray, S., & Van Speybroeck, L. 2006a, ApJ, 640, 691
19. Vikhlinin, A. 2006b, ApJ, 640, 710
20. Voit, G. M., Bryan, G. L. 2001, Nature, 2001, 414, 425